L-H transition and pedestal studies on MAST

H. Meyer[1], M.F.M De Bock[1,2], N.J. Conway[1], S.J Freethy[1,3], K. Gibson[3], J. Hiratsuka[4], A. Kirk[1], C.A. Michael[1], T. Morgan[3], R. Scannell[1], G. Naylor[1], S. Saarelma[1], A.N Saveliev[5], V.F. Shevchenko[1], W. Suttrop[6], D. Temple[1,7], R.G.L. Vann[3] and the MAST and NBI teams

[1]EURATOM/CCFE Fusion Association, Culham Science Centre, Abingdon, Oxon, OX14 3DB, UK
[2]Eindhoven Univ. of Technology, P.O. Box 513, 5600 MB Eindhoven, The Netherlands
[3]University of York, Heslington, York, YO10 5DD, UK
[4]The University of Tokyo, Kashiwa 277-8561, Japan
[5]Ioffe Institute, Politekhnicheskaya 26, 194021 St. Petersburg, Russia
[6]Max-Planck-Institute for Plasma Physics, Garching, Germany.
[7]Imperial College of Science, Technology and Medicine, London,UK.

E-mail: Hendrik.Meyer@ccfe.ac.uk

Abstract: The pedestal performance is pivotal for the success of ITER. Here, we present recent investigations on MAST focused on of L-H transition physics, pedestal transport and pedestal stability. The profile evolution of edge parameters such as the electron temperature (T_e) and density (n_e), the ion temperature (T_i, using a novel technique), the radial electric field (E_r) and the toroidal edge current density (j_ϕ, using the Motional Stark Effect) has been studied with a time resolution as fast as 0.2 ms in the case of T_e, n_e and E_r. The species dependence of the L-H power threshold, P_{LH}, was measured by comparing D and He plasmas. On MAST, P_{LH} in He is about 50% higher than in D. At the same heating powers above P_{LH} H-modes in He have a slightly narrower pedestal than in D. If the distance between the X-point and the target plates is reduced P_{LH} is lowered even in double null. The data in L-mode prior to H-mode suggest that neither the gradient nor the value of the mean T_e or E_r at the plasma edge play a major role in triggering the L-H transition. This is supported by observations of E_r and T_e made during suppression of the L-H transition with resonant magnetic field perturbations. Following the L-H transition the fluctuations are suppressed on a 5 to 10 times faster time scale than the pedestal is formed. Owing to the conductive and convective heat transport, compared to the convective particle transport, n_e evolves faster than T_e. A clear correlation of ∇T_i with collisionality is observed in H-mode. At low collisionality T_i profiles are flat with $T_i > T_e$ in the pedestal region reaching ~ 150 eV close to the separatrix. A clear increase of j_ϕ by a factor of ~ 5, of similar magnitude to the calculated bootstrap current, is observed when changing from L- to H-mode. These measurements on a ~ 2 ms time scale allow us for the first time in an ST to calculate the peeling-ballooning stability in the edge with all profiles measured. This edge stability picture used to explain edge localised modes (ELMs) breaks down for high confinement H-modes obtained with counter current NBI on MAST, where large ELMs expelling up to 7% of the plasma energy are observed despite the shallow pedestal gradients. These H-modes show an edge mode similar to the edge harmonic oscillation that suppresses the ELMs in quiescent H-mode, but without the strong well in E_r and ELMs being still present.

1. Introduction: Type-I ELMy H-mode [1] with a transport barrier at the plasma edge (ETB) is the baseline operating regime for ITER [2]. Predicting the performance of magnetically confined plasmas in future devices in the presence of this edge pedestal [3–5] due to the ETB is difficult, since the access criterion, the barrier formation and the pedestal stability are not fully understood. Hence, in the absence of predictive theory empirical scalings are used to extrapolate the performance leading to large uncertainties in particular for the transition from L-mode to H-mode (L-H transition), although heuristic models for these quantities with some predictive capability start to emerge [6, 7]. With respect to the edge localised modes (ELMs) [8, 9] the unmitigated type-I ELM is likely to be intolerable in ITER or other future devices [10]. Hence, a better understanding of the L-H transition and pedestal physics is needed calling for even better measurements to guide theory.

For both, H-mode access and the pedestal structure E_r may play an important role, since $E \times B$ flow shear stabilisation of turbulent transport [11] is believed to be the underlying physics of transport barriers. This is consistent with the general observation of strong radial electric fields during H-mode [1, 12–15]. In case of the L-H transition, there is clear evidence for the fact that an applied bias to the plasma can generate an H-mode transition [13]. However, looking at naturally occurring transition the demands on the temporal and spatial resolution are extremely high, in order to understand the causality of the L-H transition. Only a few experiments have

sufficiently good measurements to study this. A further complication is that one needs to distinguish between E_r fluctuations, $\tilde{E}_r$, and the mean equilibrium field. New results from the TJ-II stellarator suggest that it is $\tilde{E}_r$ rather than E_r that is important for the L-H transition [16]. MAST is equipped with a good set of edge diagnostics at high spatial and temporal resolution. The most important for the pedestal physics being the T_e and n_e measurements ($\Delta R = 1$ cm) using Thomson Scattering (TS)[17], the E_r and T_i measurements (3 mm $\leq \Delta R \leq$ 6 mm) using active Doppler spectroscopy [15] and the current profile measurement ($\Delta R \approx 2$ cm) using the Motional Stark Effect (MSE)[18]. The edge T_i profile uses charge exchange recombination spectroscopy between C^{6+} and $D^{\star}$. This technique has not been used before. Recent findings using this suite of edge diagnostics are discussed below.

2. H-mode access: During the non-activation phase of ITER the planned auxiliary power will be limited. Measurements on current devices suggest that the installed power will not be enough to access H-mode in H or He since $P_{LH} \propto A_{eff}^{-1}$ ($A_{eff} = \sum_\alpha M_\alpha n_\alpha / \sum_\alpha n_\alpha$) [19]. However, recent results from ASDEX Upgrade show no difference of P_{LH} between He and D discharges [20], however there is no broad experimental basis for the L-H transition in He discharges.

To study the isotope dependence on MAST discharge to discharge power scans have been performed in similar He and D plasmas (see Fig. 1). The L-H transition in He is at $t_{LH} = 0.22$ s. The D discharge enters H-mode at $t_{LH} = 0.19$ s, despite the much lower injected power of $P_{NBI} = 1.8$ MW compared to $P_{NBI} = 2.7$ MW in He. Therefore, the core temperature (Fig. 1d) is higher in He than in D, although the D discharge has a longer H-mode phase.

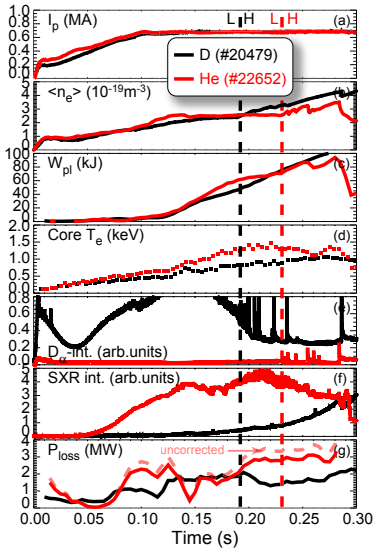

Figure 1: *Typical time traces of similar H-mode discharges in D (black) and He (red).*

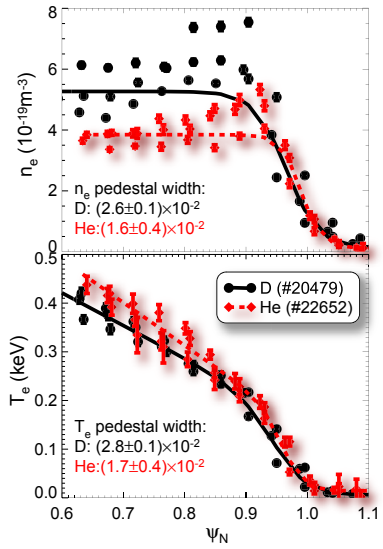

Figure 2: *Comparison of H-mode pedestal in D (black) and He (red).*

The power flowing over the separatrix, $P_{loss} = P_{abs} + P_\Omega - \partial W_{pl}/\partial t - P_{rad} \cdots$ (P_{abs}: absorbed, P_Ω: Ohmic, $P_{rad} \approx 0.1$ MW: radiated power, and $\cdots$: terms connected to the change in plasma shape that is relevant for spherical tokamaks), has to be calculated with care using TRANSP. This is for several reasons. Firstly, the He discharge still has some D inventory due to the NBI fuelling and the D captured in the wall (e.g. D_α emission in Fig. 1e). Secondly, the ratio of absorbed to injected power is lower in He compared to D. The charge exchange process between He^{2+} and D is less efficient than the process between D^+ and D. Thirdly, at high power there is evidence for enhanced ion losses/"diffusion", D_{FI}, due to the MHD driven by the fast-ion density gradient [21, 22]. Studying the sensitivity of these unknowns with TRANSP the best match with the experimental data is achieved with He to D concentration of $c_{He}/c_D \approx 0.85/0.15 \Rightarrow A_{eff} \approx 3.7$ and $D_{FI} \approx 1\ m^2/s$ leading to a correction of P_{loss} by 20% in He (see Fig. 1g).

With the same excess power $P_{loss} - P_{LH} \approx 0.3$ MW are remarkably similar (Fig. 2). The density in He discharge seems to be a little bit lower than in the D discharge with a clear density ear. The temperatures are almost the same within the error bars of the measurement, although the slope towards the core seems to be higher in He. Fitting the pedestal profiles with a modified tanh fit [23] in normalised flux space gives a pedestal width for T_e and n_e in He that is a factor of 1.6

narrower than in D. These fitted values have to be taken with caution, since the density fit needs to be corrected for the presence of the ear, and there is also a well known correlation between the fitted width and the core slope in the function used for these fits. A higher core slope leads to a narrower pedestal. The pedestal β_{pol} is very similar if calculated from the experimental profile data at the same flux surface directly. This is interesting since in He there are two dominant ion species present in the edge region rather than one in D. Also the velocity distributions is different, since dissociation is absent for He.

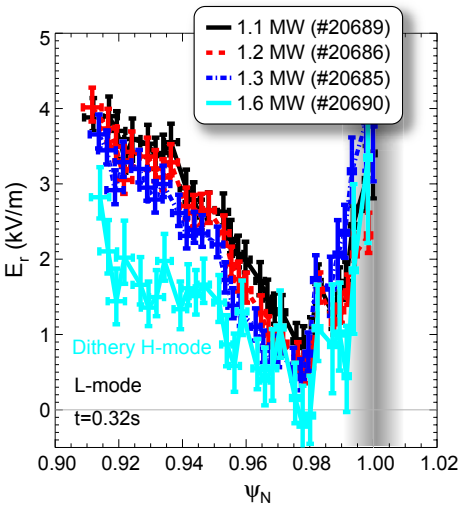

Figure 3: *Average "L-mode" edge E_r for different P_{NBI} approaching P_{LH}.*

The edge radial electric field profiles, $E_r(R)$, during the power scan in D are shown in Fig. 3. The measurements were averaged between 0.31 s $< t <$ 0.33 s, since the dithers present during this phase can't be resolved by the $\Delta t = 4$ ms individual measurement period. As H-mode is approached with increasing power little change is observed in the E_r profiles, and hence in ∇E_r. The only real difference is seen with $P_{loss} = 1.6$ MW, which samples a sustained dithering H-mode. Here, E_r starts to become more negative. This data suggest that the DC ∇E_r may not play a key role for the L-H transition. This is supported by several data discussed below including fast measurements through a L-H transition. It should be noted however, that these mostly L-mode discharges already show a considerable ∇E_r.

On JET it was found that the distance between the X-point and the strike points sensitively affects H-mode access [24]. On MAST also a sensitive dependence on the distance between the outer strike point and the X-point was observed [25] in single null (SN) plasmas. Initial power threshold measurements in a pair of down shifted lower SN discharges ($I_p = 0.8$ MA, $\bar{n}_e = (2.4 \pm 0.1) \cdot 10^{19}$ m^{-3}, $B_t = -0.55$ T) with $Z_{mag} = -0.2$ m and $Z_{mag} = -0.1$ m show a difference in P_{LH} of about a factor 2 with $P_{LH} = (1.3 \pm 0.2)$ MW and $P_{LH} = (2.6 \pm 0.2)$ MW for the lower and upper discharge respectively. Unfortunately, these lower SN discharges experience small sawtooth crashes every 20 ms $< \Delta t <$ 30 ms with slightly different characteristics. In both cases the L-H transition is triggered by a sawtooth crash. P_{LH} is chosen between the two values of P_{loss} that lead to a sustained H-mode after the crash. This effect on H-mode access with X-point height is also present in double null (DN). Here the elongation needs to be changed to change Z_x. As can be seen from Fig. 4 the higher κ discharge has a clear L-H transition at $t_{LH} = 0.3$ s at a power level where the lower κ discharge is still in L-mode, albeit close to H-mode. In order to get an H-mode of similar quality in the lower κ shape the power has to be increased by $\Delta P_{NBI} = 0.2$ MW. Parameters at the L-H transition for the 4 different shapes are given in table 1.

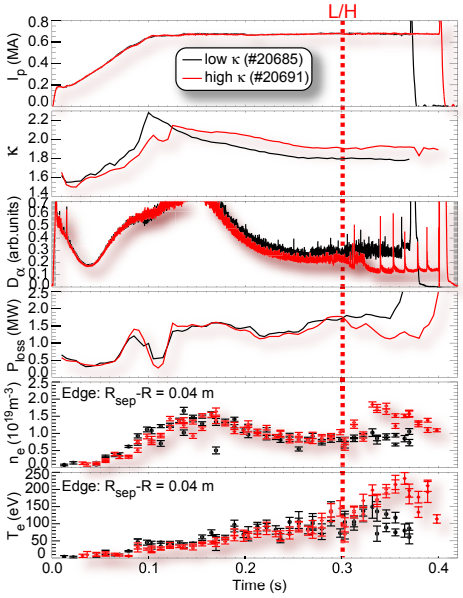

Figure 4: *Comparison of typical time traces between two discharges with different κ at the same input power.*

A comparison of the L-mode E_r at lower power shows no significant change between low and high κ (Fig. 5) supporting the notion that the mean E_r is not the driving factor in the L-H transition. During the application of resonant magnetic perturbations (RMP) P_{LH} is increased

Z_{mag} (m)	R_x (m)	Z_x (m)	P_{LH} (MW)	$\bar{n}_e$ (10^{19}m^{-3})	S_{pl} (m^2)	δ_l	δ_u	κ	q_{95}	L_c (m)
0.21	0.58	−1.25	1.3	2.5	21.5	0.44	0.18	1.67	3.5	13
0.10	0.59	−1.12	2.6	2.3	21.6	0.39	0.26	1.71	3.8	12
0.0	0.57	1.12	<1.8	2.7	24.5	0.42	0.42	1.91	6.6	16
0.0	0.57	1.04	1.8	2.6	23.4	0.42	0.42	1.80	5.5	13

Table 1: *Discharge parameters for X-point P_{LH} scan ($\delta_{l,u}$: lower/upper triangularity, S_{pl}: plasma surface, L_c SOL connection length from mid-plane to the outer divertor plate).*

and E_r becomes more positive [26]. This would be consistent with a decreased $E \times B$ leading to a loss of H-mode with RMPs. However, increasing the power to regain H-mode access does not change E_r. There is also no change of n_e or T_e close to the edge prior to the L-H transition as can be seen from the lower two panels in Fig. 4 showing the values at $R - R_{sep} = -4$ cm. Hence, there is no evidence for a critical T_e needed to access H-mode as favoured by many L-H transition theories (see also Fig. 7).

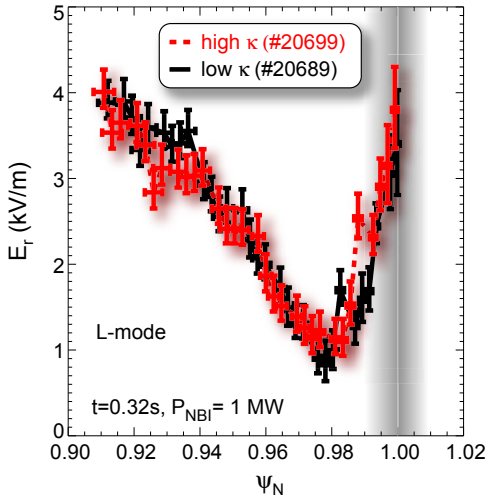

Figure 5: *Comparison of edge E_r for high (red) and low κ (black) in L-mode close to the L-H transition.*

Surprisingly the SN discharge with the higher X-point has the shorter connection length, L_c, due to the slight differences in shape. It is unlikely that such a small change in L_c is responsible for the large difference in P_{LH}. The change in L_c with κ is also small. It is remarkable how small changes in the shape can sensitively influence the conditions to access H-mode. A close examination of all profiles is needed to see which local parameters may be responsible for these changes.

3. Pedestal Formation: To improve the understanding of the H-mode access and the pedestal formation fast measurements $\Delta t = 0.2$ ms of E_r, T_e, and n_e have been performed. Using the dependence of the H-mode access on the magnetic configuration [25] a sequence of L-H, H-L, and L-H transitions was triggered in synchronisation with the 8 TS profiles 0.2 ms apart every 33 ms ($\Delta t_{las} \approx 10$ ns). This lead to a natural jitter of the individual transitions of less than 3ms greatly improving the statistics. E_r was measured at four radial positions and the development during the L-H transition and through an ELM can be seen in Fig. 6. Each L-H transition starts with 1 – 3 dithers. Prior to the transition there is no discernible change in E_r. In detail, the Lorentz term $E_r^L = u_\phi B_\theta - u_\theta B_\phi$ seems to correlate with the drops in D_α that indicate the better confinement, whereas the diamagnetic term $E_r^D = \partial_r p/(eZn)$ seems to show an anti-correlation. This is until the last dither when E_r^D becomes more positive close to the separatrix and more negative further inward. E_r^L becomes more negative over the whole measured region. In total this leads to an increased positive gradient in E_r with the shear layer forming around $R - R_{sep} \approx -1.2$ cm. The increase of $\partial_r E_r$ happens on similar time scales as the decrease of D_α with $E_r \Delta t/\Delta E_r \approx 0.6$ ms for the innermost chord. The dynamic of the E_r^L differs slightly from E_r^D in the sense that the more inner radii show larger changes than the outer radii with E_r^D showing, if at all, the opposite behaviour. The ELM completely destroys this shear layer during its rise time (Fig. 6b). It should be noted that the time points are marked at the *end* of the acquisition interval.

As can be seen from Figures 7 and 8 there is a clear increase of n_e and $|\nabla n_e|$ after the L-H transition at the edge with a typical rise time of $n_e \Delta t/\Delta n_e \approx 3$ ms. T_e hardly changes,

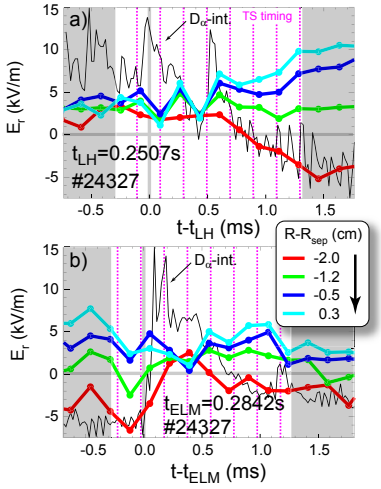

Figure 6: *Evolution of E_r through (a) an L-H transition and (b) an ELM.*

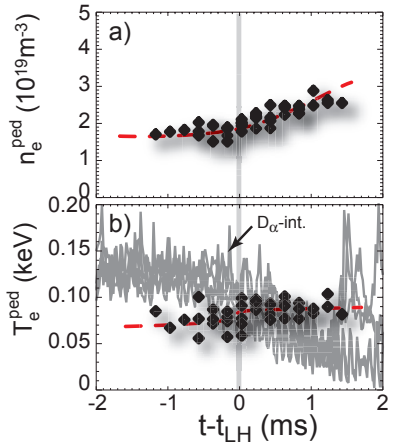

Figure 7: *Evolution of (a) n_e and (b) T_e through various L-H transitions.*

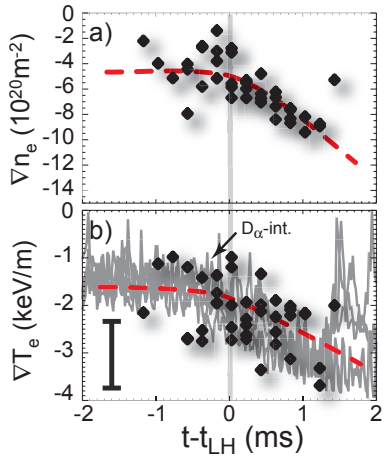

Figure 8: *Evolution of (a) ∇n_e and (b) ∇T_e through various L-H transitions*

but $|\nabla T_e|$ seems to increase as well although the statistical uncertainty indicated in the plot (bottom left in Fig. 8) is large. Such behaviour could be either due to the initial formation of a particle barrier rather than a thermal barrier, or by the formation of an ion barrier with $n_e(t)$ reflecting the evolution of n_i. Analysis of the visible light fluctuations show that the edge turbulence is suppressed in less than 100 μs, which is at least 5 times faster than the evolution observed in E_r, T_e or n_e. This suggests that the measured profiles evolve as a consequence of the suppressed turbulent transport rather than the changes causing the turbulence suppression. Further statistical analysis is needed to verify this. In Figs. 7, 8, t_{LH} is defined at the top of the last dither to get a unique time for multiple shots corrensponding to $t - t_{LH} \approx 0.5$ ms in Fig. 6.

Novel Charge exchange measurements using the reaction $C^{6+} + D^* \rightarrow C^{5+} + D^+$ in a thermal D_2 beam provides T_i on a 10 ms – 20 ms time scale with high spatial resolution 3 mm $< \Delta R <$ 6 mm. At low collisionality $\partial_r T_i$ is very flat, and high temperatures similar to the pedestal temperature $T_i < 150$ eV are measured right up to the separatrix. A good correlation of $\partial_r T_i$ with collisionality is observed. This is consistent with the fact that in hot MAST pedestals the ions are in the banana regime with $\rho_{pol,i} \approx 15$ mm of the order of the width of the T_e pedestal. According to a very general argument about the conservation of entropy in the pedestal one expects $\rho_{pol,i} \nabla \ln T_i \ll 1 \Rightarrow \rho_{pol,i} \ll L_{T_i}$ [27]. As the plasma becomes more collisional entropy is conserved within each flux surface and a stronger gradient in T_i can exist. This is supported by the MAST measurements shown in Fig. 9

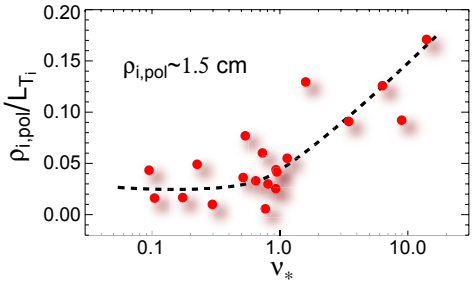

Figure 9: *Collisionality dependence of $\rho_{pol,i}/L_{T_i}$ in MAST H-modes.*

4. Pedestal Stability The most common model for the trigger of type-I ELMs is the onset of peeling-ballooning modes [28] with experimental points often sitting close to the stability boundary calculated numerically from the pedestal profiles. Here, generally $p_e = p_i$ is assumed and the bootstrap current is calculated according to neoclassical theory [29]. The new T_i measurements on MAST suggest that $p_e = p_i$ is only viable at high collisionality, where the pedestal is typically far from the MHD stability boundary. At low collisionality $T_i > T_e$ in the pedestal pressor gradient region. The impact of this, however, is probably small since $\partial_r p_i = k_B(n_i \partial_r T_i + T_i \partial_r n_i)$ with the first term decreasing, whilst the second term increases. Large ELM like bursts encountered in MAST H-mode discharges with counter current NBI, however,

do no fit the peeling-ballooning model since hardly any pedestal exists to destabilise ELMs. Nevertheless, the instability structurally indistinguishable from a type-I or type-III ELM ejects 2 kJ $\leq \Delta W \leq$ 6 kJ of the stored energy. This is $\Delta W/W_{\mathrm{pl}} < 7\%$ with respect to the total stored energy and $\Delta W/W_{\mathrm{ped}} < 30\%$ ($W_{\mathrm{ped}} \approx 20$ kJ), which more like the energy loss observed during type-I rather than type-III ELMs.

A more fundamental question for pedestal stability is if the edge current is calculated correctly. Unfortunately, the edge current density j_ϕ usually derived from a pitch angle, $\gamma_m = \arctan(B_\theta/B_\phi)$, measurement is very hard to measure, since generally the integrated quantity γ_m is not only small at the tokamak edge where $B_\phi \gg B_\theta$, but the change due to the edge current is minimal. Furthermore, the few existing measurements of the local B_θ have to poor a time resolution to resolve the ELM cycle [30]. In the ST, the strong field line pitch on the low field side leads to measurable changes in γ_m [31] using the Motional Stark Effect (MSE) measurement ($\Delta t = 2$ ms, $\Delta R \approx 2$ cm) [18].

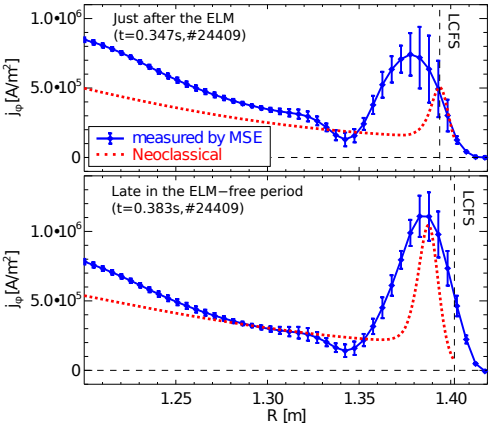

Figure 10: *Comparison of j_ϕ from MSE with the neoclassical calculation according to Sauter et.al. [29]*

Consistent with the picture of pressure driven edge current, strong edge currents are observed in H-mode as can be seen from Fig. 10 showing the comparison between j_ϕ derived from MSE and j_ϕ based on the neoclassical calculation of the bootstrap current [29]. Again the assumptions $T_{\mathrm{i}} = T_{\mathrm{e}}$ and $n_{\mathrm{i}} = n_{\mathrm{e}}$ are used. Profiles are shown just after the ELM ($t = 0.347$ s) and late in the ELM-free period. It is clear that in both cases the neoclassical calculation predicts less edge current than measured by MSE. The difference is most noticeable just after the ELM where the calculated peak in j_ϕ is both more narrow and lower than j_ϕ measured by MSE. Late in the ELM-free period the height of the j_ϕ peak is similar for both the neoclassical calculation and the measurement, but as the width is smaller the total edge current is less. The wider profile is possibly caused by the low spatial resolution compared to the pedestal width (see below and Fig. 12). In this case the integrated current would be distributed in a narrower region leading to an even higher j_ϕ leading to the conclusen that the used expressions from neoclassical theory are incomplete. For example, the edge E_r could lead to an enhancement of j_ϕ [32], or the assumption that $\rho_i \ll L_\perp$ (with ρ_i the ion gyro radius and $L_\perp$ the gradient length) could account for the discrepancies. Also, a bootstrap calculation assumes the plasma to be in equilibrium, which, especially just after the ELM crash, might not be the case.

Interestingly j_ϕ is not affected by the occurrence of a type-I ELM. In the particular case measured j_ϕ was rising before the ELM, and keeps doing so after the ELM for several ms, whereas as expected $\max(|\nabla p_{\mathrm{e}}|)$ does drop significantly at the ELM crash. A delay due to current diffusion on resistive time scales seems insufficient to explain this. Also $\max(j_\phi)$ sometimes decreases whilst $\max(|\nabla p_e|)$ increases. This may be due to an increase $\nu_\star$, as the increase in $|\nabla p_{\mathrm{e}}|$ is mainly due to an increase in n_{e}, which reduces the bootstrap fraction of the edge current [33].

Figure 11 shows a $\max(j_\phi)$ versus $\max(|\nabla p_{\mathrm{e}}|)$ stability plot. The 2 dashed lines indicate the ballooning

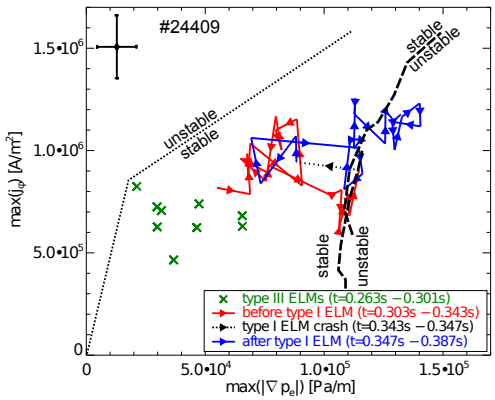

Figure 11: *Measured trajectory of $\max(j_\phi)$ versus $\max(|\nabla p_{\mathrm{e}}|)$ in comparison with the stability limits calculated with ELITE.*

stability boundary for the time points $t = 0.343$ s and $t = 0.383$ s. These boundaries are indicative only, as they will differ for each time point due to profile shape changes. No unstable peeling modes were found in the simulations at these times. To guide the eye a dotted line is added to the figure indicating were the peeling boundary is expected. During the type III ELMy phase of the discharge $\max(j_\phi)$ and $\max(|\nabla p_e|)$ are located in the area where the peeling boundary is expected (crosses). In the first long ELM free period, $\max(j_\phi)$ and $\max(|\nabla p_e|)$ start near the peeling boundary, but a sudden increase in $\max(|\nabla p_e|)$ brings the data points to the ballooning boundary. As $\max(|\nabla p_e|)$ increases $\max(j_\phi)$ shows an initial decrease, but it recovers when $\max(|\nabla p_e|)$ stabilises. Interestingly it is not just the data point right before the ELM crash that lies on the stability boundary; the plasma lingers around the stability boundary for several ms before the ELM crash. At the ELM crash $\max(|\nabla p_e|)$ drops while $\max(j_\phi)$ stays more or less the same. The second ELM free period is similar to the first one: a sudden increase of $\max(|\nabla p_e|)$, with a slight drop in $\max(j_\phi)$, followed by an increase of both $\max(|\nabla p_e|)$ and $\max(j_\phi)$. This time the data points even cross the ballooning boundary well before the ELM crash. However, the position of the ballooning boundary is almost within the errors bars of $\max(j_\phi)$ and $\max(|\nabla p_e|)$ (see top left of the figure). More j_ϕ makes the plasma more unstable.

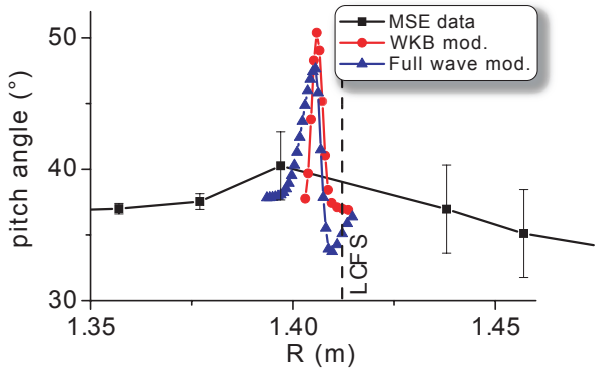

Figure 12: *Pitch angle derived from the analysis of 2-D electron Bernstein emission.*

The pitch angle can also be derived by the analysis of 2-D electron Bernstein wave emission (EBE)[34]. A pitch angle profile from a prototype system in ELM-free H-mode in comparison with the MSE measurement is shown in Fig. 12. The spatial resolution of the EBE measurement is indeed much higher than for the MSE measurement, but the integrated profile is consistent with MSE. The good localisation is given by the strong n_e gradient at the edge measured using TS. This data suggests that j_ϕ in MAST is much higher than can be accounted for by standard neoclassical theory. Of particular interest is that the γ_m profile requires a negative current sheath close to the separatrix. Such a current sheath may suppress the turbulence [35]. Currently a 36 antenna imaging system is under development, which should be able the measure γ_m on sub ms timescales, possibly resolving ELMs.

5. Conclusions The MAST studies of H-mode access, pedestal formation and stability give unique insight into the underlying physics. The L-H power threshold in He on MAST is about 50% higher than in D. H-mode access is greatly influenced by the vertical position of the X-point in single null and double null (change of κ). It is not likely, that the small changes of the outer scrape-off-layer connection length are responsible for the observed differences. The more positive radial electric field at the edge due to the application of resonant magnetic perturbations may explain the higher power threshold observed in these plasmas, but the data from the power scan, change of κ and fast measurements through the L-H transition suggest that the mean field is only a secondary player for the transition. In MAST $T_i > T_e$ in the pedestal with flat gradients at low collisionality, since the large banana orbits couple the flux surfaces in the pedestal together with respect to entropy conservation. With increasing collisionality this coupling is broken and $|\nabla T_i|$ increases. No clear change in n_e, T_e, and E_r or their gradients is observed prior to the L-H transition. Comparing the evolution of E_r, n_e, ∇E_r, ∇n_e and ∇T_e after the transition with that of the fluctuations suggest that the profiles react on a relatively sudden change in the transport rather than causing the transition.

Measurements of the detailed time evolution ($\Delta t = 2$ ms) of the edge current density, j_ϕ in

inter ELM periods using the Motional Stark Effect (MSE) suggest that the peeling-ballooning model for the type-I ELM onset may be incomplete, although the measurements are in broad agreement with ideal MHD stability calculations. This is supported by the edge stability in counter current NBI H-modes that show large ELM like instabilities with almost no pedestal. The measured edge current density exceeds the neoclassical prediction by more than a factor of two, in particular after an ELM crash. This is supported by the analysis of 2-D electron Bernstein wave emission (EBE). a novel technique, showing that the $\Delta R = 2$ cm resolution of the MSE measurement is probably not enough to resolve the edge current layer on MAST. This data also suggests that j_ϕ changes sign close to the separatrix. Future innovative improvements of the EBE system (next year) should allow fast measurements of j_ϕ possibly through an ELM.

Acknowledgements: This work was funded by the RCUK Energy Programme under grant EP/G003955 and the European Communities under the Contract of Association between EURATOM and CCFE. The views and opinions expressed herein do not necessarily reflect those of the European Commission.

References

[1] WAGNER, F., Plasma Phys. Control. Fusion **49** (2007) B1.
[2] IKEDA, K., Nuclear Fusion **47** (2007) S1.
[3] ASDEX-TEAM, Nucl. Fusion **29** (1989) 1959.
[4] KIRK, A. et al., Plasma Phys. Contr. Fusion **46** (2004) 551.
[5] MAGGI, C., Nuclear Fusion **50** (2010) 066001.
[6] FUNDAMENSKI, W. et al., A new model for the L-H transition in tokamaks, Presentation to the JET Task force E (14/09/2010) to be published.
[7] SNYDER, P. et al., Nucl. Fusion **49** (2009) 085035 (8pp).
[8] ZOHM, H., Plasma Phys. Control. Fusion **38** (1996) 105.
[9] KIRK, A. et al., Plasma Phys. Contr. Fusion **47** (2005) 315.
[10] LOARTE, A. et al., Plasma Phys. Control. Fusion **45** (2003) 1549.
[11] TERRY, P. W., Rev. Mod. Phys. **72** (2000) 109.
[12] BURRELL, K. H., Phys. of Plasmas **6** (1999) 4418, Invited contribution to the APS-meeting 1999 in Atlanta.
[13] WEYNANTS, R. R. et al., Plasma Phys. Control. Fusion **40** (1998) 635.
[14] MEYER, H. et al., Czechoslovak Journal of Physics **50** (2000) 1451.
[15] MEYER, H. et al., Journ. Phys.: Conf. Series **123** (2008) 012005.
[16] ESTRADA, T. et al., Plasma Phys. Control. Fusion **51** (2009) 124015 (11pp).
[17] SCANNELL, R. et al., Rev. Sci. Instr. **77** (2006) 10E510.
[18] CONWAY, N. et al., Rev. Sci. Instr. **81** (2010), accepted.
[19] RIGHI, E. et al., Nucl. Fusion **39** (1999) 309.
[20] RYTER, F. et al., Nucl. Fusion **49** (2009) 062003 (4pp).
[21] MEYER, H. et al., Nuclear Fusion **49** (2009) 104017 (13pp).
[22] TURNYANSKIY, M. et al., Nuclear Fusion **49** (2009) 065002 (9pp).
[23] GROEBNER, R. J. et al., Plasma Phys. Control. Fusion **40** (1998) 673.
[24] ANDREW, Y. et al., Plasma Phys. Control. Fusion **46** (2004) A87.
[25] MEYER, H. et al., Plasma Phys. Contr. Fusion **50** (2008) 015005.
[26] KIRK, A. et al., Magnetic perturbation experiments on MAST using internal coils, EXD/8-2 at 23rd IAEA Fusion Energy Conference, Daejeon, Korea 11-16 Oct., 2010.
[27] KAGAN, G. et al., Plasma Physics and Controlled Fusion **50** (2008) 085010 (25pp).
[28] WILSON, H. R. et al., Phys. of Plasmas **9** (2002) 1277.
[29] SAUTER, O. et al., Phys. of Plasmas **9** (2002) 5140.
[30] THOMAS, D. M. et al., Phys. Rev. Lett. **93** (2004) 065003.
[31] BOCK, M. D. et al., Measurements of the edge current evolution during MAST H-modes using MSE, submitted to Phys. Rev. Lett.
[32] KAGAN, G. et al., Phys. Rev. Lett. **105** (2010) 045002.
[33] THOMAS, D. M. et al., Plasma Physics and Controlled Fusion **48** (2006) A183.
[34] SHEVCHENKO, V. F. et al., Fusion Science and Technology (2011), accepted.
[35] PETVIASHVILI, V., Plamsa Physics Reports **20** (1994) 265.